European Journal of Inorganic Chemistry

Supporting Information

# Atomically Precise Rhodium-Gold Carbonyl Nanoclusters: In-Depth Synthesis and Multivalence Investigation of $[Rh_{16}Au_6(CO)_{36}]^{6-}$, and its Correlation with $[Rh_{10}Au(CO)_{26}]^{3-}$

Silvia Ruggieri, Guido Bussoli, Marco Bortoluzzi, Cristiana Cesari, Tiziana Funaioli, Stefano Zacchini, Maria Carmela Iapalucci,* and Cristina Femoni*

**Atomically Precise Rhodium-Gold Carbonyl Nanoclusters: In-Depth Synthesis and Multivalence Investigation of $[Rh_{16}Au_6(CO)_{36}]^{6-}$, and its Correlation with $[Rh_{10}Au(CO)_{26}]^{3-}$.**

Silvia Ruggieri,[a],[b] Guido Bussoli,[a] Marco Bortoluzzi,[c] Cristiana Cesari,[a] Tiziana Funaioli,[d] Stefano Zacchini,[a] Maria Carmela Iapalucci,*[a] and Cristina Femoni*[a]

[a] Department of Industrial Chemistry "Toso Montanari", University of Bologna, Via Gobetti 85, 40129 Bologna, Italy

[b] Laboratory of Luminescent Materials, Department of Biotechnology, University of Verona and INSTM, UdR Verona, Strada Le Grazie 15, 37134 Verona, Italy

[c] Department of Molecular Sciences and Nanosystems, Ca' Foscari University of Venice, Via Torino 155, 30170 Mestre (VE), Italy

[d] Department of Chemistry and Industrial Chemistry, University of Pisa, Via Moruzzi 13, 56124 Pisa, Italy

## SUPPORTING INFORMATION

### LIST OF CONTENT

**IR and ESI mass spectra for $[Rh_{16}Au_6(CO)_{36}]^{6-}$ (1).**

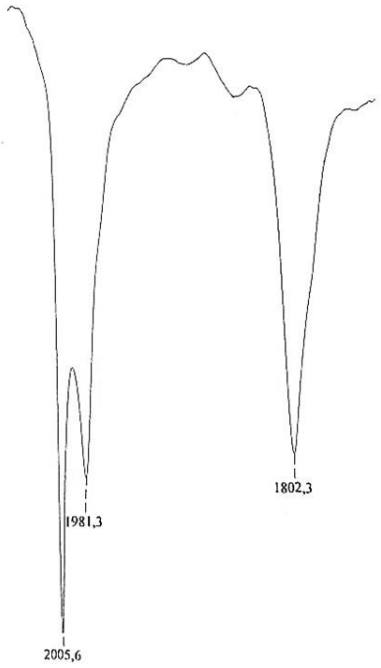


**Figure S1a**. IR spectrum of $[Rh_{16}Au_6(CO)_{36}][TEA]_6$ registered in $CH_3CN$ solution.

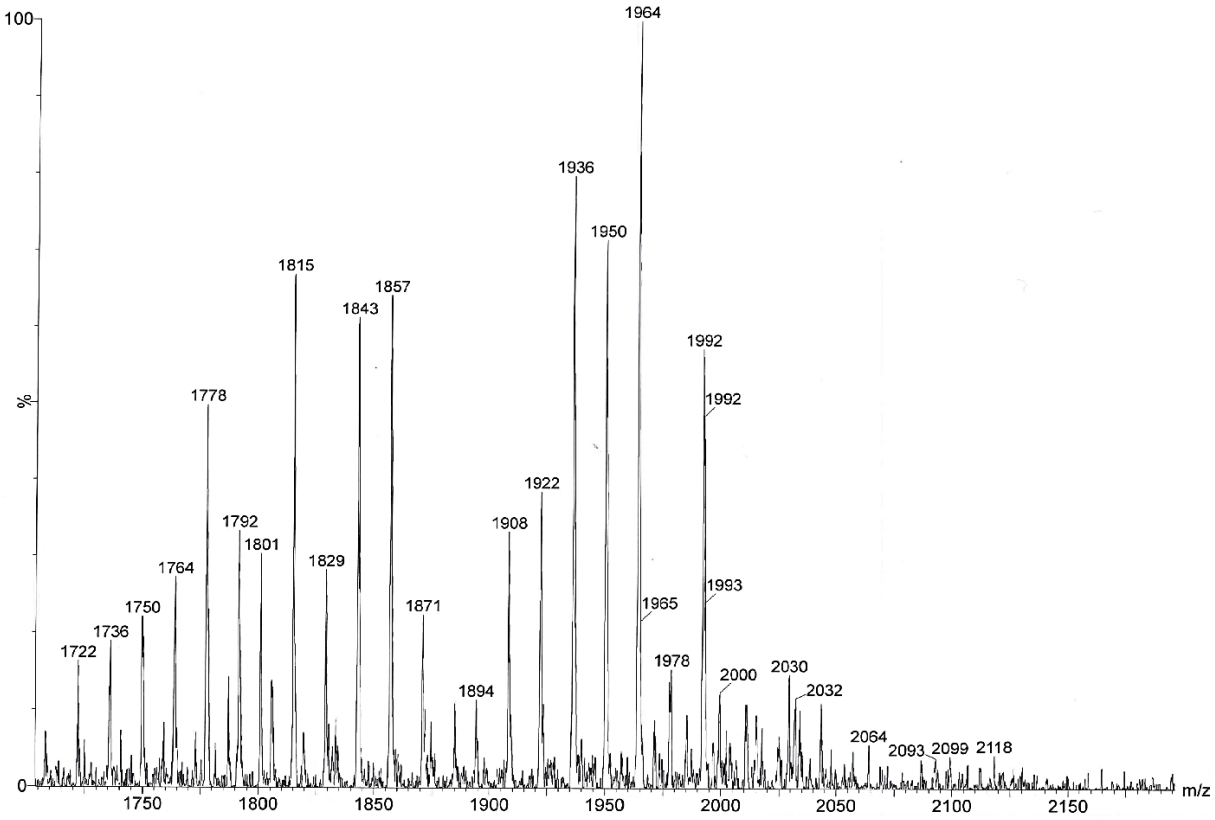


**Figure S1b**. ESI-MS spectrum of the *2*− region of $[Rh_{16}Au_6(CO)_{36}][TEA]_6$.

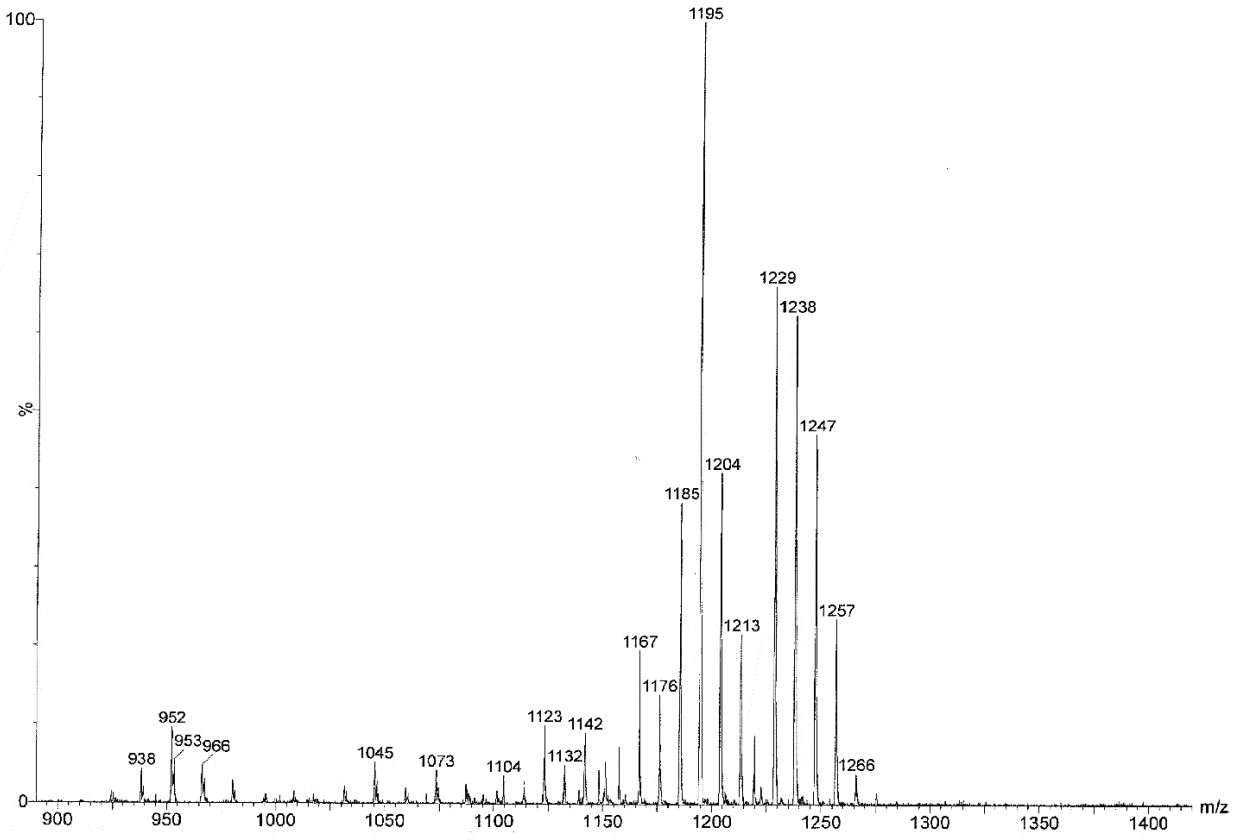


**Figure S1c**. ESI-MS spectrum of the *3*− region of $[Rh_{16}Au_6(CO)_{36}][TEA]_6$.

| ***Signals / group of signals (m/z)*** | ***Corresponding ions*** |
|---|---|
| *1992-1978-1964-1950-1936-1922-1908-1894* | $\{[Rh_{16}Au_6(CO)_{32\text{-}31\text{-}30\text{-}29\text{-}28\text{-}27\text{-}26\text{-}25}][TEA]_2\}^{2-}$ |
| *1871-1857-1843-1829-1815-1801* | $\{[Rh_{16}Au_6(CO)_{28\text{-}27\text{-}26\text{-}25\text{-}24\text{-}23}][TEA]\}^{2-}$ |
| *1792-1778-1764-1750-1736-1722* | $[Rh_{16}Au_6(CO)_{27\text{-}26\text{-}25\text{-}24\text{-}23\text{-}22}]^{2-}$ |
| *1266-1257-1247-1238-1229* | $\{[Rh_{16}Au_6(CO)_{30\text{-}29\text{-}28\text{-}27\text{-}26}][TEA]\}^{3-}$ |
| *1213-1204-1195-1185-1176-1167* | $[Rh_{16}Au_6(CO)_{29\text{-}28\text{-}27\text{-}26\text{-}25\text{-}24}]^{3-}$ |

**Table S1a**. ESI-MS peak assignments for $[Rh_{16}Au_6(CO)_{36}][TEA]_6$.

**Spectroelectrochemical Experiments**

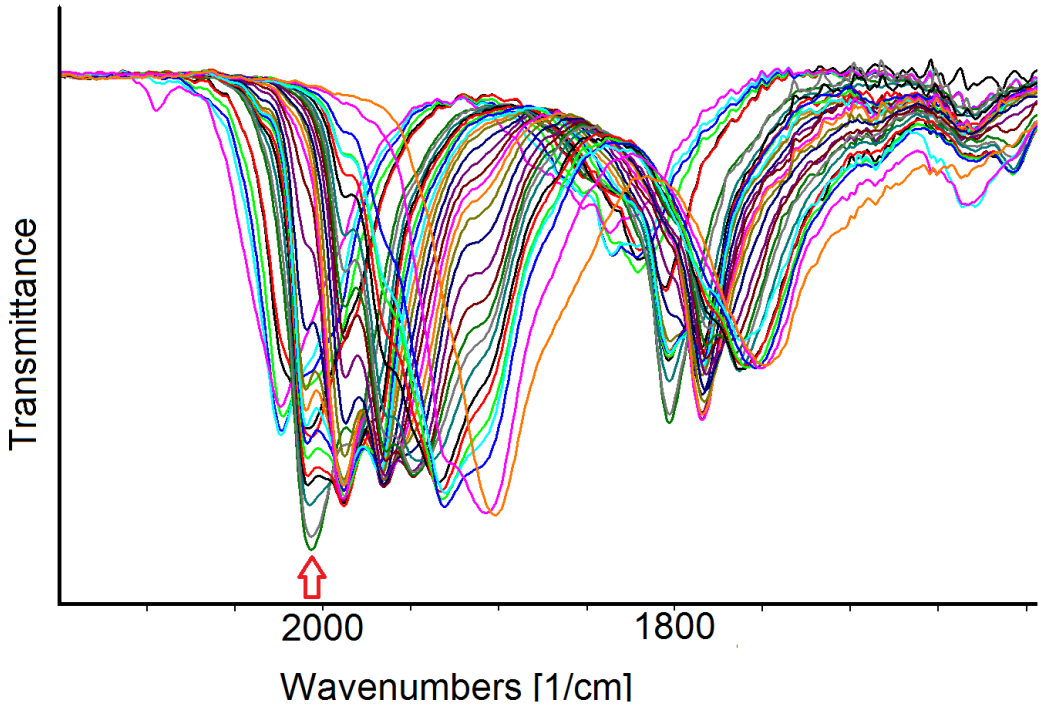


**Figure S1d.** Infrared spectra of $[Rh_{16}Au_6(CO)_{36}]^{6-}$ recorded in an OTTLE cell during a slow WE potential scan between –0.5 to –2.0 V in $CH_3CN$ containing 0.1 mol $dm^{-3}$ [TBA][$PF_6$], under CO atmosphere. The solvent and supporting electrolyte absorptions have been subtracted. The red arrow indicates the initial spectrum.

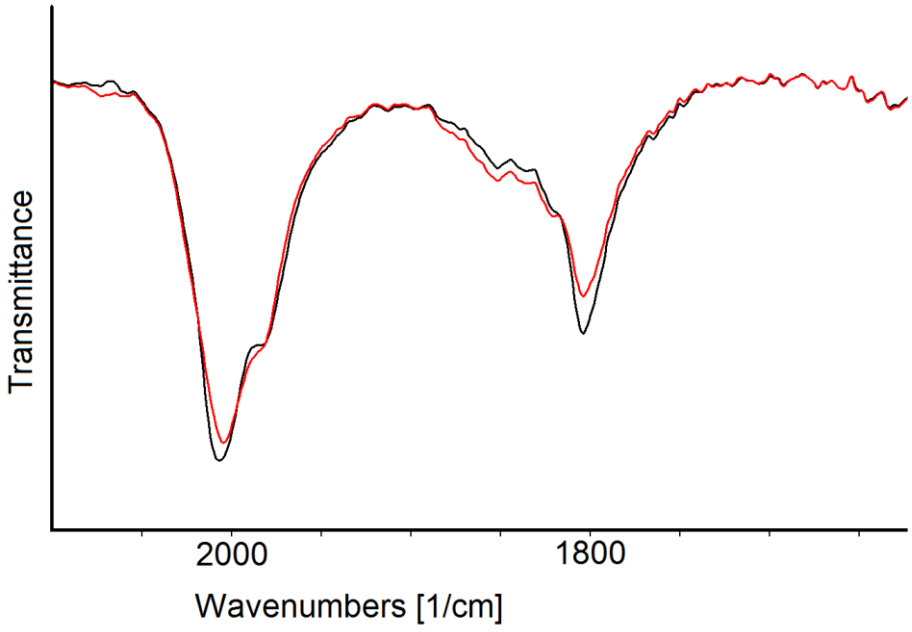


**Figure S1e**. IR spectra of a $CH_3CN$ solution of $[Rh_{16}Au_6(CO)_{36}]^{6-}$ recorded in an OTTLE cell before (black line) and after (red line) a cyclic voltammetry between –0.8 to –0.3 V (scan rate 1 mV $s^{-1}$), under CO atmosphere. [TBA][$PF_6$] (0.1 mol $dm^{-3}$) as the supporting electrolyte. The solvent and supporting electrolyte absorptions have been subtracted.

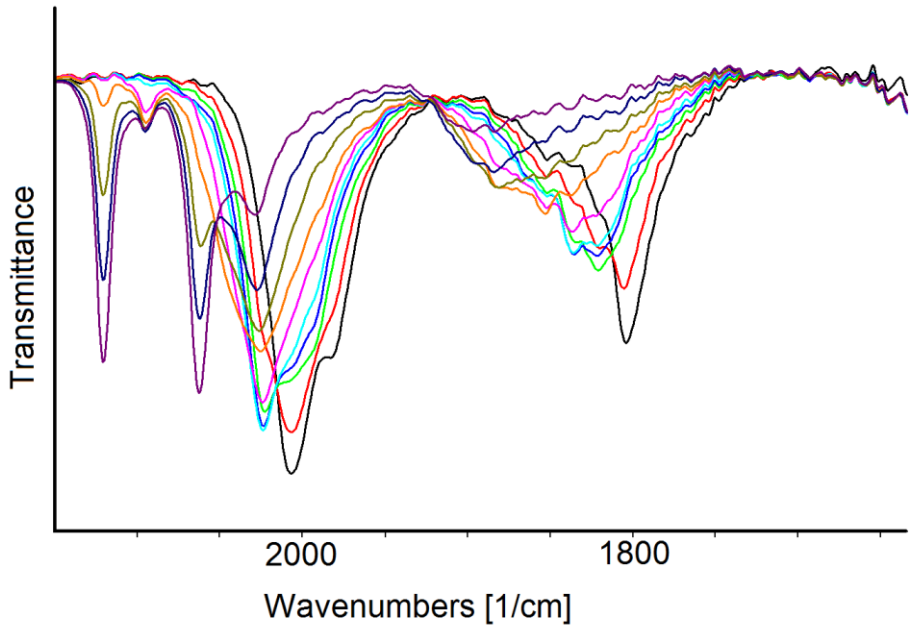


**Figure S1f**. Infrared spectra of $[Rh_{16}Au_6(CO)_{36}]^{6-}$ recorded in an OTTLE cell during the progressive increase of the working electrode potential E from –0.8 to +0.2 V in $CH_3CN$ containing 0.1 mol $dm^{-3}$ [TBA][$PF_6$], under CO atmosphere. The solvent and supporting electrolyte absorptions have been subtracted.

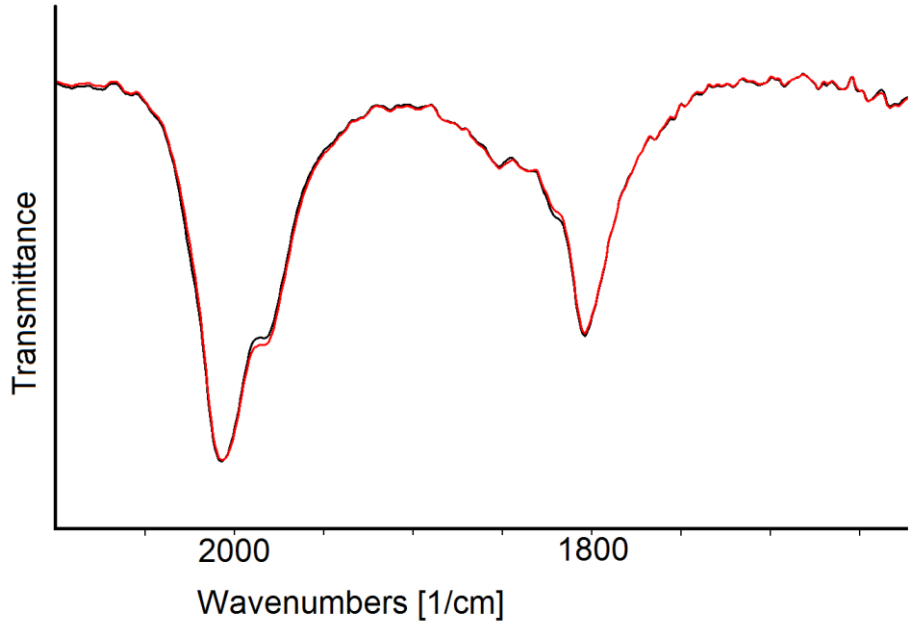


**Figure S1g.** IR spectra of a $CH_3CN$ solution of $[Rh_{16}Au_6(CO)_{36}]^{6-}$ recorded in an OTTLE cell before (black line) and after (red line) a cyclic voltammetry between –0.8 to –1.4 V (scan rate 1 mV $s^{-1}$), under CO atmosphere. [TBA][$PF_6$] (0.1 mol $dm^{-3}$) as the supporting electrolyte. The solvent and supporting electrolyte absorptions have been subtracted.

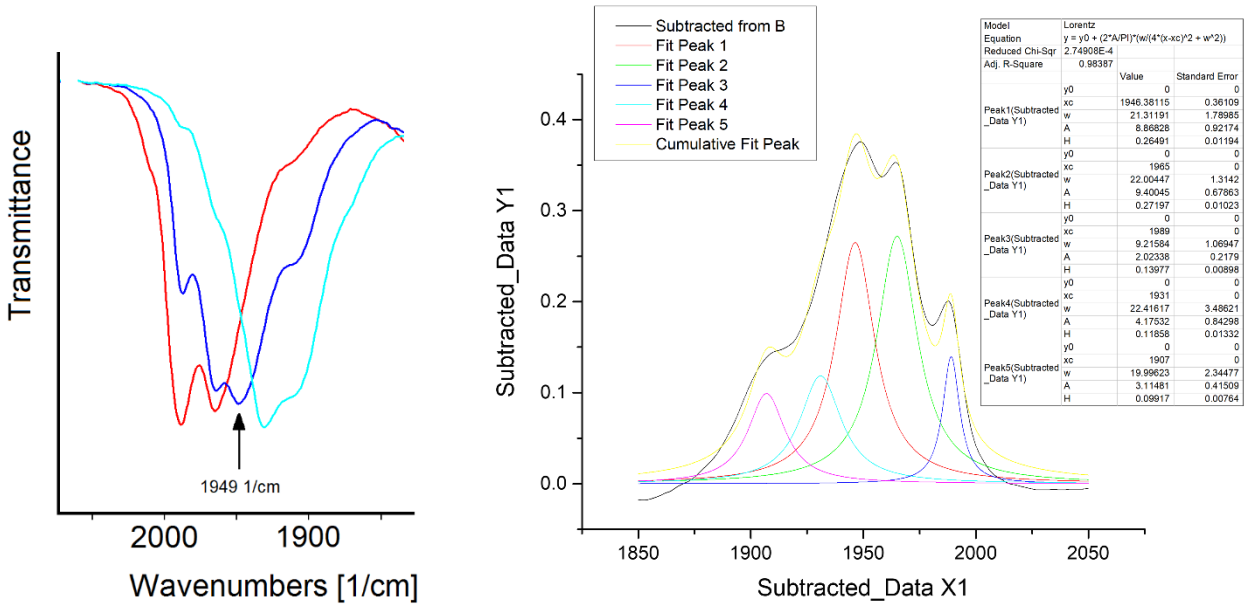


(a) (b)

**Figure S1h**. (a) First (red line), intermediate (blue line) and final (turquoise line) spectra in the second reduction sequence of $[Rh_{16}Au_6(CO)_{36}]^{6-}$ registered during the progressive potential decrease from –1.4 to –1.7 V (Figure 8c). (b) Spectral deconvolution of the intermediate IR spectrum (blue line in (a)). Its contribution is matched by the combination of main separate bands at 1989, 1965, 1931 and 1907 $cm^{-1}$, corresponding to red and turquoise curves, respectively and of a new band at 1946 $cm^{-1}$ band due to the now unravelled -8 negative charge.

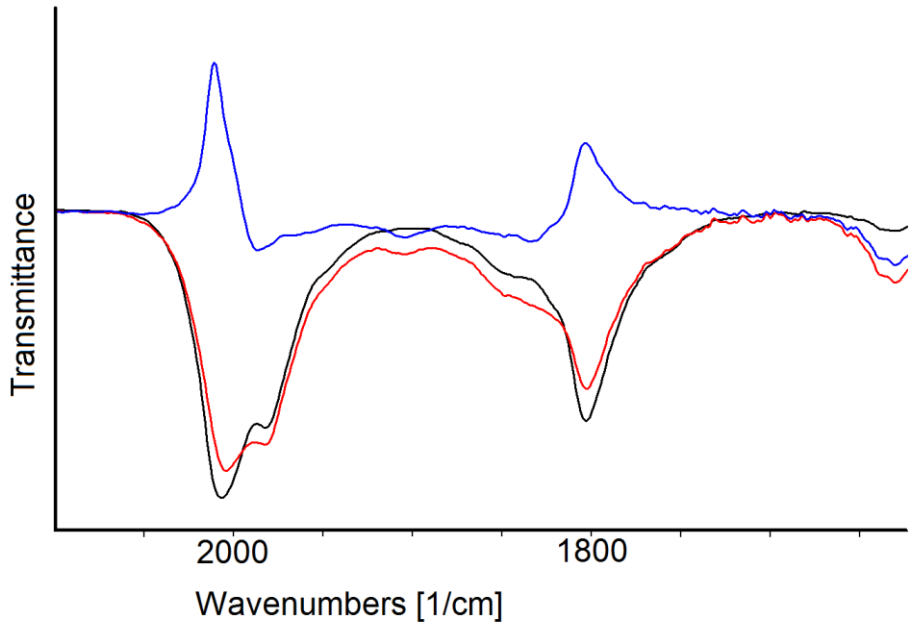


**Figure S1i**. IR spectra of a $CH_3CN$ solution of $[Rh_{16}Au_6(CO)_{36}]^{6-}$ recorded in an OTTLE cell before (black line) and after (red line) a cyclic voltammetry between –1.4 to –1.7 V (scan rate 1 mV $s^{-1}$). The blue line represents their difference spectrum. [TBA][$PF_6$] (0.1 mol $dm^{-3}$) as the supporting electrolyte. The solvent and supporting electrolyte absorptions have been subtracted.

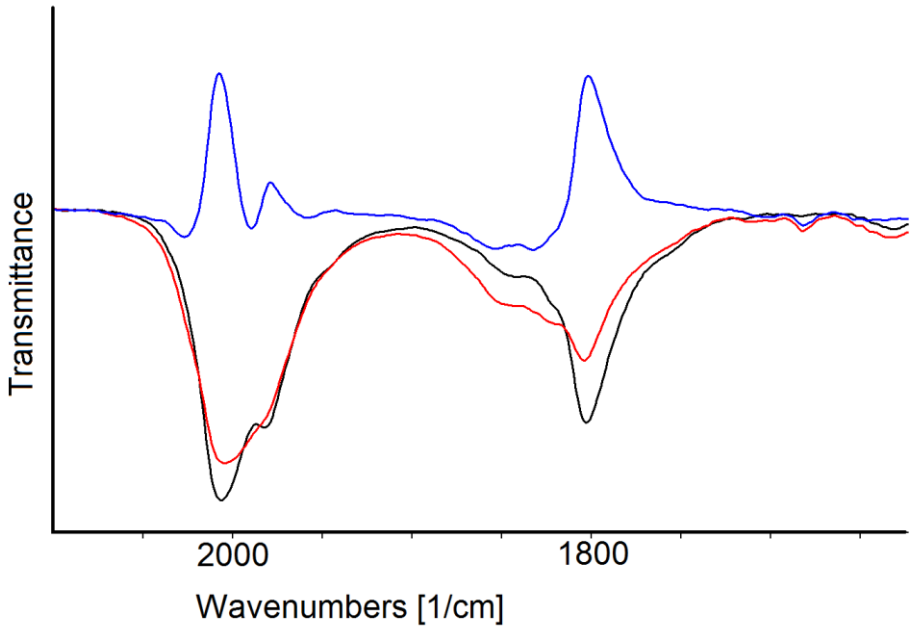


**Figure S1l**. IR spectra of a $CH_3CN$ solution of $[Rh_{16}Au_6(CO)_{36}]^{6-}$ recorded in an OTTLE cell before (black line) and after (red line) a cyclic voltammetry between –1.7 to –2.0 V (scan rate 1 mV $s^{-1}$). The blue line represents their difference spectrum. [TBA][$PF_6$] (0.1 mol $dm^{-3}$) as the supporting electrolyte. The solvent and supporting electrolyte absorptions have been subtracted.

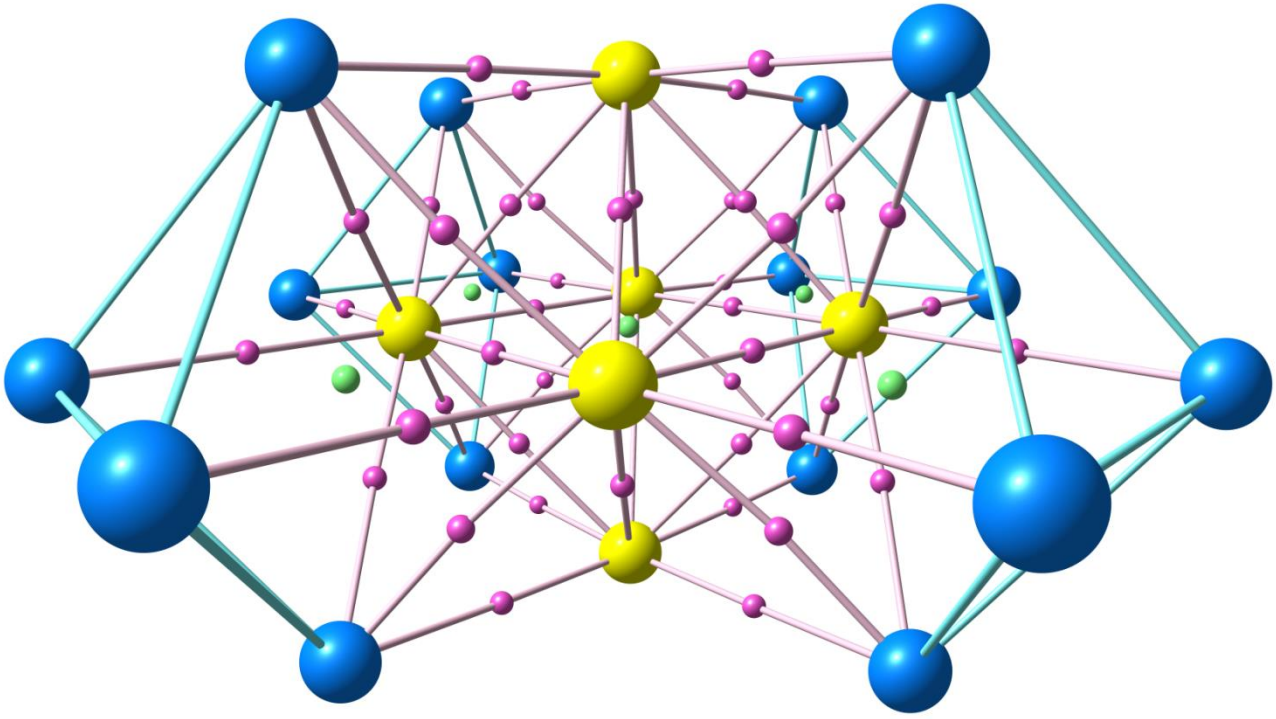

**Figure S1m**. *$Au_6Rh_{16}$* core of $[Rh_{16}Au_6(CO)_{36}]^{6-}$ with (3,-1) BCPs (pink small spheres) and selected (3,+3) CCPs (green small spheres). Rh atoms are in blue, Au atoms in yellow.

**Table S1b**. Average properties at selected (3,-1) BCPs and (3,+3) CCPs computed for $[Rh_{16}Au_6(CO)_{36}]^{n-}$ (n = 5, 6, 7) clusters.

| **n** | ρ (e Å$^{-3}$) | V (hartree Å$^{-3}$) | E (hartree Å$^{-3}$) | $\nabla^2\rho$ (e Å$^{-5}$) |
|---|---|---|---|---|
| *(3,-1) Au---Au* | | | | |
| **7** | 0.232 | -0.206 | -0.029 | 2.129 |
| **6** | 0.236 | -0.212 | -0.029 | 2.197 |
| **5** | 0.227 | -0.202 | -0.026 | 2.143 |
| *(3,-1) Au---Rh* | | | | |
| **7** | 0.257 | -0.240 | -0.047 | 2.090 |
| **6** | 0.262 | -0.246 | -0.048 | 2.130 |
| **5** | 0.263 | -0.252 | -0.049 | 2.204 |
| *(3,+3) $Au_6$* | | | | |
| **7** | 0.085 | -0.043 | -0.001 | 0.583 |
| **6** | 0.092 | -0.047 | -0.002 | 0.623 |
| **5** | 0.089 | -0.044 | -0.002 | 0.577 |
| *(3,+3) $Rh_4Au_2$* | | | | |
| **7** | 0.131 | -0.060 | -0.006 | 0.701 |
| **6** | 0.134 | -0.064 | -0.006 | 0.749 |
| **5** | 0.138 | -0.065 | -0.006 | 0.736 |

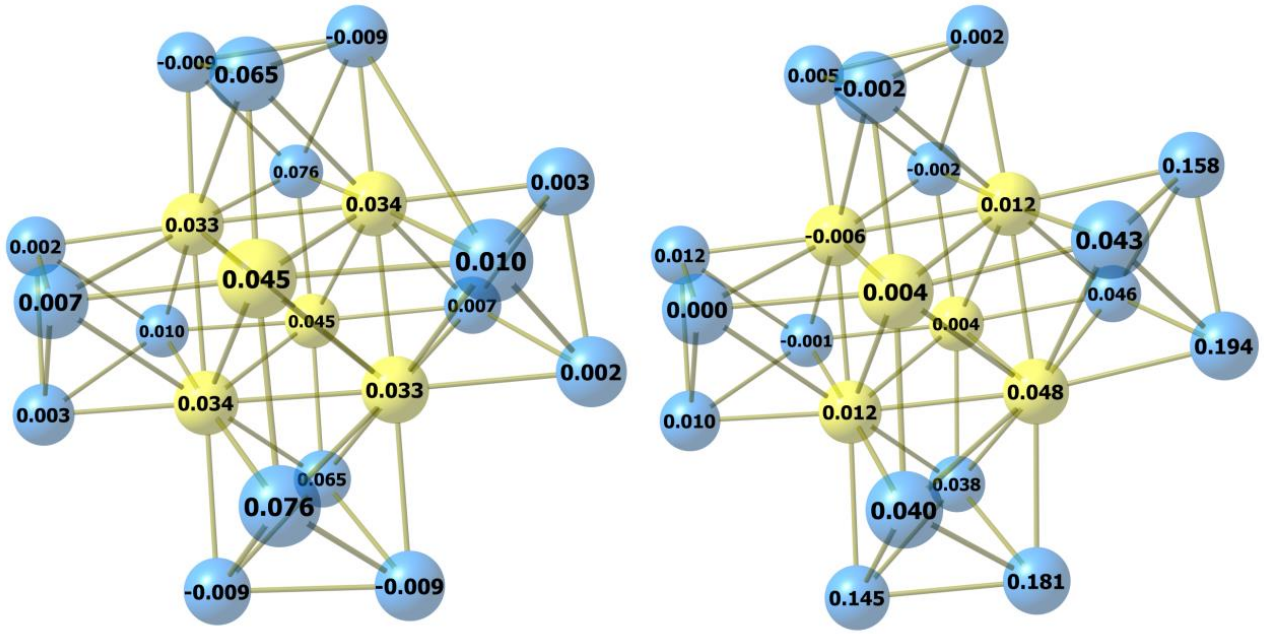


**Figure S1n**. *Au₆Rh₁₆* cores of $[Rh_{16}Au_6(CO)_{36}]^{5-}$ and $[Rh_{16}Au_6(CO)_{36}]^{7-}$ with values of Löwdin spin population (a.u.). Rh atoms are in blue, Au atoms in yellow.

**IR and ESI mass spectra for $[Rh_{10}Au(CO)_{26}]^{3-}$ (2).**

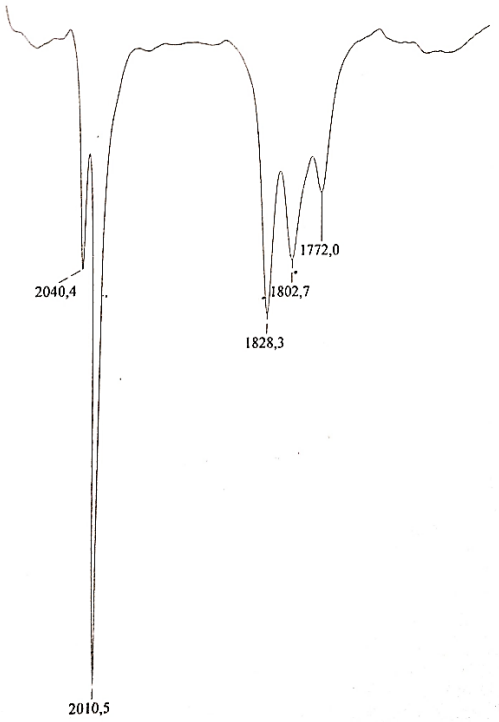


**Figure S2a**. IR spectrum of $[Rh_{10}Au(CO)_{26}][TBMA]_3$ registered in $CH_3CN$ solution.

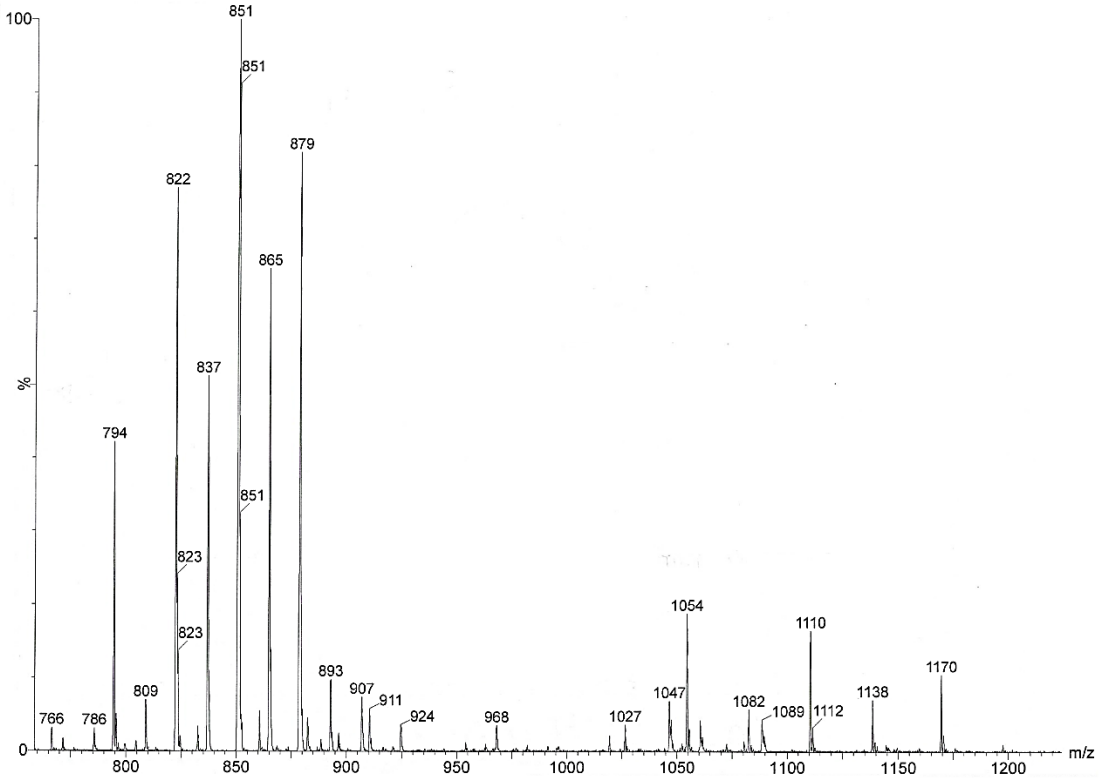

**Figure S2b**. ESI-MS spectrum of $[Rh_{10}Au(CO)_{26}][TBMA]_3$ registered in $CH_3CN$ solution (higher m/z region).

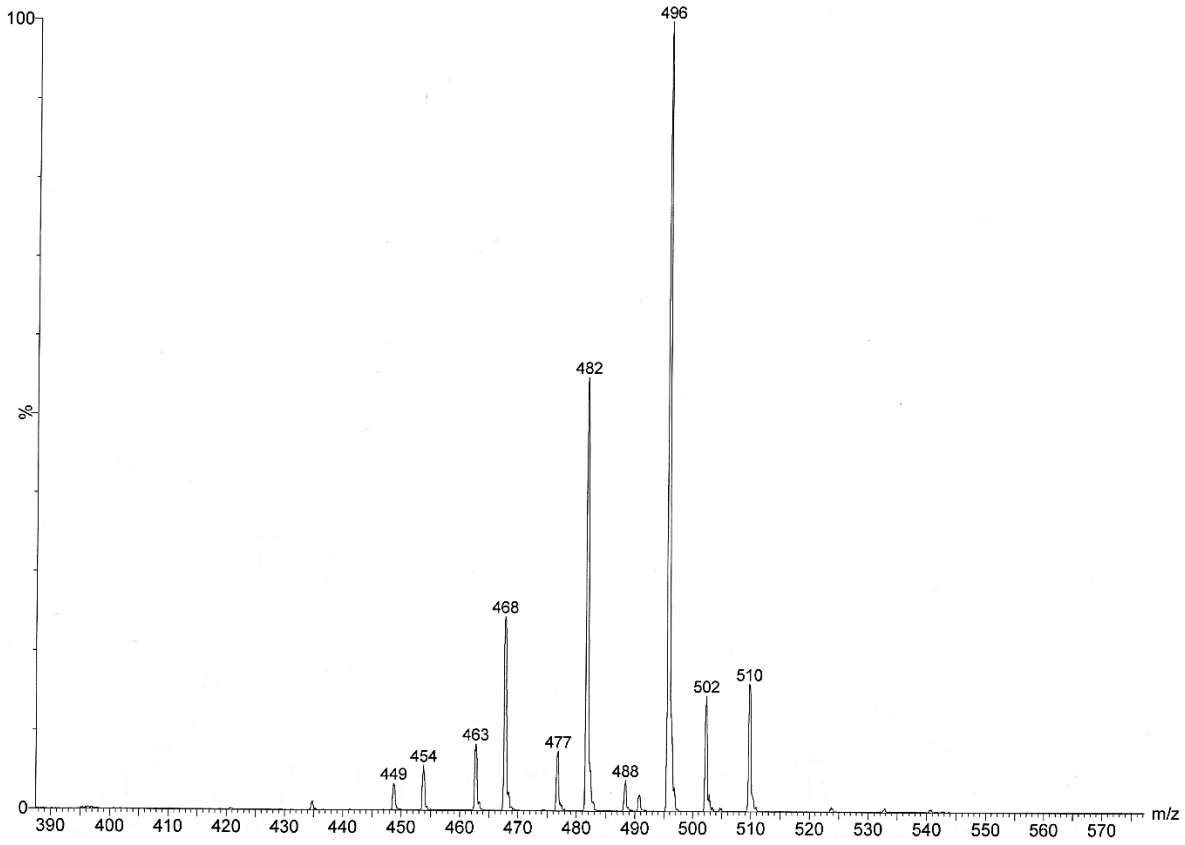


**Figure S2c**. ESI-MS spectra of $[Rh_{10}Au(CO)_{26}][TBMA]_3$ registered in $CH_3CN$ solution (lower m/z region).

| ***Signals or group of signals (m/z)*** | ***Corresponding ions*** |
|---|---|
| *1170* | $\{[Rh_5Au(CO)_{11}][TBMA]\}^-$ |
| *1138-1110-1082-1054* | $[Rh_5Au(CO)_{14\text{-}13\text{-}12\text{-}11}Cl]^-$ |
| *968* | $\{[Rh_{10}Au(CO)_{20}][TBMA]\}^{2-}$ |
| *907-893-879-865-851-837-822-808* | $[Rh_{10}Au(CO)_{21\text{-}20\text{-}19\text{-}18\text{-}17\text{-}16\text{-}15\text{-}14}]^{2-}$ |
| *510-496-482-468-454* | $[Rh_5Au(CO)_{11\text{-}10\text{-}9\text{-}8\text{-}7}]^{2-}$ |

**Table S2a.** ESI-MS peak assignments for $[Rh_{10}Au(CO)_{26}][TBMA]_3$.

**Table S2b.** Crystallographic data for cluster **2**

| | |
|---|---|
| Formula | $C_{56}H_{48}AuN_3O_{28}Rh_{10}$ |
| Fw | 2405.04 |
| Crystal system | Monoclinic |
| Space group | $P2_1/n$ |
| a (Å) | 18.6419(9) |
| b (Å) | 14.5075(7) |
| c (Å) | 25.1273(12) |
| $\alpha$ (°) | 90 |
| $\beta$ (°) | 105.386(2) |
| $\gamma$ (°) | 90 |
| Cell volume (Å$^3$) | 6552.1(5) |
| Z | 4 |
| D (g/cm$^3$) | 2.438 |
| $\mu$ (mm$^{-1}$) | 4.761 |
| F(000) | 4568 |
| θ limits (deg) | 1.580 to 25.000 |
| Index ranges | −22<=h<=22, −17<=k<=17, −29<=l<=29 |
| Reflections collected | 84774 |
| Independent reflections | 11530 [R(int) = 0.1065] |
| Completeness to θ max | 99.9% |
| Data/restraints/parameters | 11530 / 576 / 874 |
| Goodness of fit | 1.231 |
| $R_1$ (I > 2σ(I)) | 0.0669 |
| $wR_2$ (all data) | 0.1227 |
| Largest diff. peak and hole, e Å$^{-3}$ | 2.122 and -2.182 |

**Table S2c:** Bond lengths (Å) from crystallographic analyses

| | |
|---|---|
| Au(1)-Rh(5) | 2.7135(10) |
| Au(1)-Rh(11) | 2.7168(11) |
| Au(1)-Rh(4) | 2.7244(10) |
| Au(1)-Rh(3) | 2.7389(10) |
| Au(1)-Rh(8) | 2.7430(10) |
| Au(1)-Rh(7) | 2.7497(11) |
| Au(1)-Rh(6) | 2.7592(11) |
| Au(1)-Rh(9) | 2.7899(10) |
| Rh(2)-Rh(3) | 2.8837(13) |
| Rh(2)-Rh(6) | 2.8855(13) |
| Rh(2)-Rh(5) | 2.8910(13) |
| Rh(2)-Rh(7) | 2.9177(13) |

| | |
|---|---|
| Rh(3)-Rh(5) | 2.9481(13) |
| Rh(3)-Rh(6) | 2.9494(13) |
| Rh(4)-Rh(10) | 2.8626(13) |
| Rh(4)-Rh(9) | 2.9367(14) |
| Rh(4)-Rh(11) | 2.9679(14) |
| Rh(5)-Rh(7) | 2.9597(13) |
| Rh(6)-Rh(7) | 2.9409(13) |
| Rh(8)-Rh(10) | 2.9025(13) |
| Rh(8)-Rh(9) | 2.9239(13) |
| Rh(8)-Rh(11) | 2.9698(13) |
| Rh(9)-Rh(10) | 2.9016(13) |
| Rh(10)-Rh(11) | 2.8708(13) |